Composition-dependent microstructure evolution in liquid MgCl$_2$-KCl: A first-principles molecular dynamics study

Wenshuo Liang, Guimin Lu *, Jianguo Yu

School of Resources and Environmental Engineering, East China University of Science and Technology, Shanghai 200237, China
National Engineering Research Center for Integrated Utilization of Salt Lake Resource, East China University of Science and Technology, Shanghai 200237, China

A B S T R A C T

The structural evolution of MgCl$_2$-based materials is of considerable interest due to their current and potential applications in numerous technologies, such as electrolyte in magnesium electrolysis, secondary coolant for high-temperature reactors, and a new generation heat transfer fluid for concentrated solar power systems. However, their intrinsic feature is poorly understood and difficult to obtain with experimental techniques. In this work, first-principles molecular dynamics simulations (FPMD) are adopted to investigate the structural evolution of molten MgCl$_2$-KCl fused salt. Examination of the radial distribution function, probability distribution of coordination numbers and bond angle distribution of the melts reveals that the local geometry of the Mg converts from mainly tetrahedral to a distorted octahedral with one-two anion vacancies as the concentration of MgCl$_2$ is increased. Accompanied by this structural change, there are also corresponding variations in the stability and dynamics of the system. Further analysis of the stability and the lifetime of the Mg—Cl bond indicate that the coordinated Cl$^-$ anions around Mg^{2+} cations are more dynamic in MgCl$_2$ richer compositions. Moreover, this study shows that the addition of MgCl$_2$ will inhibited the formation of isolated structural units and promote the extension of Mg chains. In conclusion, the simulations successfully reproduce the structural features of MgCl$_2$-KCl melts and highlight the application prospects of FPMD simulations in revealing the local structure of molten salts.

© 2020 Published by Elsevier B.V.

1. Introduction

Nowadays, it is still an attractive issue to explore the microstructure and its evolution of MgCl$_2$-based molten salts. These salts are mainly used as electrolytes in the electrolysis process, in which magnesium chloride is decomposed into magnesium and chlorine. In actual engineering applications, MgCl$_2$ can not be used alone because of its characteristics of a high melting point, low electrical conductivity, and being easy to hydrolyze. Generally, magnesium electrolytes are complex and pluralistic systems, in which KCl, NaCl, and CaCl$_2$ are frequently added [1]. The additives complicate the structures of the electrolytes, thus resulting in changes in the electrochemical behavior and physicochemical properties of the electrolytes. The optimization of components is commonly a practical way to improve the performance of electrolytes, which implies that it is often empirical and at an engineering level. Unlike aluminum electrolyte, in-depth studies of magnesium electrolytes are very limited. Therefore, the structural evolution of magnesium electrolytes has not been researched systematically. In addition, a deep

knowledge of the intrinsic feature of MgCl$_2$-based materials is required for the correct interpretation of their spectroscopic data [2,3]. In conclusion, there is a growing need for a general method to explain and predict the microstructure evolution of MgCl$_2$-based materials.

The ability to examine structural evolution at an atomic level may contribute to a better design of the electrolyte formula and an in-depth understanding of electrochemical behavior. The density functional theory based first-principles molecular dynamics simulations, which computes the forces acting on the nuclei from electronic structure calculations, are successfully employed to study thermodynamic properties of many kinds of molten salts and effectively reproduces their structural characteristics observed in experiments [4–10]. Most recently, FPMD simulations were employed to study the ionic structure and transport properties of KF–NaF–AlF$_3$ fused salt [11–13], and the evolution of [UCl$_6$]$^{n-}$ ($n = 2, 3$) groups in UCl$_n$-NaCl ($n = 3,4$) systems [14]. FPMD simulations extremely enriched our understanding of the characteristics of molten salts. Despite its obvious advantages, it should be noted that a price has to be paid for performing FPMD simulations: the simulation cell and simulation time are much smaller than what is affordable by classical molecular dynamics.

In previous works [15–19], systematic results of molten alkali chlorides have been presented from MD simulations. More recently, we

have performed some initial exploratory calculations on pure $MgCl_2$ using FPMD simulations [20]. In practical terms, molten salt mixtures are of far greater commercial significance because their performance can be improved by adjusting the composition. Accurate structural information is helpful for us to understand and predict such characteristics. However, for the $MgCl_2$-ACl (where A is an alkali metal) molten salts, the variation trends with the composition of the local structures have not been uncovered yet, which deserve in-depth study.

In this paper, a representative $MgCl_2$-ACl molten salt $MgCl_2$-KCl is studied using FPMD simulations. First, details of the computational method for simulating $MgCl_2$-KCl molten salt by FPMD are illustrated. In the results and discussion section, the effect of $MgCl_2$ concentration on the structural evolution is addressed and compared with the experimental measurements to verify our FPMD results on molten $MgCl_2$-KCl.

2. Computational methods

The Vienna Ab Initio Simulation Package (VASP) [21,22] based on density functional theory (DFT) is employed for our FPMD simulations. The Perdew-Burke-Ernzerhof (PBE) [23] functional of the generalized gradient approximation (GGA) is used for the electron exchange-correlation. The projector augmented wave (PAW) [24,25] method has been employed for all the ion-electron interactions. The Mg $3s^2$ electrons, K $3s^2 3p^6 4s^1$, electrons and Cl $3s^2 3p^5$ electrons are explicitly regarded as valence electrons. The kinetic energy cutoff of 600 eV and a $1 \times 1 \times 1$ k-point mesh is chosen for FPMD simulations. We note that the energy cutoff of 600 eV, adopted here and in previous work [20], is not the best choice,which will definitely increase the cost of calculation and limit the choice of a larger simulation cell. Therefore, a value of 420 eV will be chosen in future research.

The initial configurations of 22.22, 33.33, 50.00 and 80.00 mol% $MgCl_2$ with KCl were generated by packing ions randomly into given simulation cells using the Packmol code [26]. A series of simulation cells containing 140 atoms were prepared and their volumes were primarily estimated by the experimental density at a particular temperature. Each of the simulation cells was launched at 2000 K to initially equilibrate the initial configurations. It was feasible to create converged liquid structures from high-temperature calculations within timescales of up to 10 ps at 2000 K with FPMD. RDFs showed that randomly placed ions by Packmol were arranged in the form of ordered states(see Fig. S1 in the supporting information). Then the high-temperature liquids were quenched at a rate of 180 K/ps to 1073 K. After these runs, the equilibrium volume was optimized at five fixed volumes for each particular composition. For each fixed volume, the total pressure (P) is evaluated as the average of the last 90% of a 6 ps simulation. Starting from the quenched liquids, 6 ps duration in FPMD is found to be long enough to reach the convergence of energy and pressure(Fig. S2). For each composition, the total pressures were fitted to a third-order Birch–Murnaghan equation of state [27,28] (Fig. S3), and the equilibrium volume was evaluated as the cell volume corresponding to zero pressure. Finally, FPMD simulation was carried out for 20 ps at this equilibrium volume for the following analysis of structure and transport properties. A time step of 1 fs was adopted to reduce the energy drift.

It has been shown previously that the GGA/PBE exchange-correlation functional will significantly overestimate the equilibrium volume for molten salt systems, and the addition of van der Waals (vdW) dispersion interaction will lower this overestimation [5,6]. Therefore, the semi-empirical DFT-D2 of Grimme [29,30] is introduced in this work.

This research was conducted with a very small system since FPMD calculations are very computationally intensive. Nevertheless, we think it is acceptable compared with FPMD simulations reported in literatures [6,7,9,14]. All FPMD simulations, apart from the quenching process, are done in the NVT ensemble using a Nosé-thermostat with periodic boundary conditions. The analysis of the static structure, including radial distribution function, bond angle distribution and

structure factor, is conducted by the R.I.N.G.S. [31] code, and the cage correlation function is computed using MDAnalysis code [32].

3. Results and discussion

3.1. Validation of simulation results

3.1.1. Structure factors

The static structure factor S(q) is calculated for $MgCl_2$-KCl mixtures to further verify the simulation results. The S(q) is calculated through the following equation

$$S(q) = \frac{1}{N} \sum_{jk} b_j b_k \left\langle e^{iq[r_j - r_k]} \right\rangle \tag{1}$$

where b_j and r_j represent respectively the X-rays scattering length and the position of the atom j. N represents the total number of atoms in the system studied. The X-rays scattering is q point dependent with $b_j = f_j(q)$, see reference [33] for details.

We previously calculated the structural factor of pure magnesium chloride, which matches well with the neutron scattering data obtained by Biggin and Enderby. Fig. 1 shows static structure factors of the $MgCl_2$-KCl melts at 1073 K for each component. The calculated S(q) for KCl-50.00%$MgCl_2$ and KCl-33.33%$MgCl_2$ matches well with the X-ray scattering data of Fei Wu et al. [34], which provides confidence in our following analysis. In addition, it can be seen that an FSDP occurs at roughly 1Å and appears predominantly in the structure factors, especially at high $MgCl_2$ concentrations. The appearance of this FSDP is believed to be a direct manifestation of network formation. And it is generally associated with intermediate-range order (IRO) on a length scale substantially larger than the sum of any ionic radii. Besides, it can be observed that the addition of $MgCl_2$ results in a smoothly increasing of the FSDP intensity in S(q). This finding is also in agreement with recent X-ray scattering experiments and MD simulations of molten $MgCl_2$-KCl [34], which exhibits a similar trend of the height of FSDP with $MgCl_2$ concentration. The underlying cause of this increment is well discussed in the work by Fei Wu et al. [34]: The across-network correlations of Mg^{2+} complex that does not belong to the same network
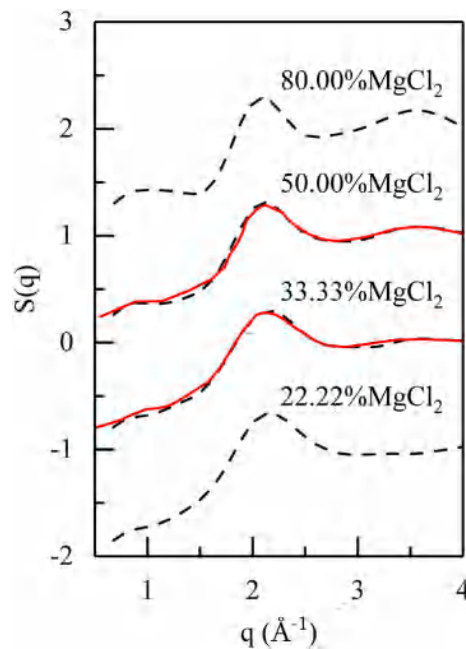

Fig. 1. The static structure factor S(q) for $MgCl_2$-KCl mixtures at various $MgCl_2$ concentrations. S(q) from our FPMD simulations are marked in black (dashes).X-ray scattering data of KCl-50.00%$MgCl_2$ and KCl-35.00%$MgCl_2$ from reference [34] (red).
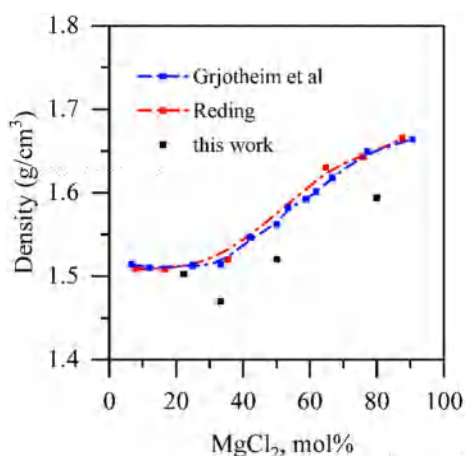
Fig. 2. Calculated density for MgCl$_2$-KCl fused salts from purely FPMD simulations with the NVT ensemble at 1073 K as a function of MgCl$_2$ concentration.

play a significant role on the origin of the FSDP. And the addition of MgCl$_2$ into the MgCl$_2$-KCl mixtures will result in a larger density of such across network correlations, and, finally, lead to an increment of the intensity of FPSD in S(q).

3.1.2. Density

Fig. 2 shows that the densities of MgCl$_2$-KCl melts derived from the equilibrium volumes. For the molten MgCl$_2$-KCl mixtures, the calculated densities increase from 1.470 to 1.594 g cm^{-3} as the concentration of MgCl$_2$ increased from 22.22 to 80.00 mol%. Meanwhile, the experimental density obtained by Reding [35] and Grjotheim [36] increased from 1.508 to 1.657 g/cm^{-3} and 1.515 to 1.650 g/cm^{-3}, respectively. FPMD densities for MgCl$_2$-KCl are underestimated with the deviation between 0.37 and 3.80% compared to the experiments, suggesting a slight underestimation of the interionic interaction in MgCl$_2$-KCl fused salt by the

PBE exchange-correlation functional with DFT-D2 method. The local structure of ionic species that we analyze in this work is largely determined by the short-range interactions, and hence, a slight underestimation of the density should not affect the principal results of this work significantly. Although the NPT dynamics, using the method of Parrinello and Rahman [37,38], is now available in VASP, it shows a larger error in calculated equilibrium volumes than that devised from NVT calculations when compared with experimental values [39].

3.2. Local structure of the MgCl$_2$-KCl system

3.2.1. Radial distribution function

The partial radial distribution function (RDF) is used to study the local structure of magnesium atom in the fused salt, and the RDF was defined as

$$g_{\alpha\beta}(r) = \frac{1}{4\pi\rho_\beta r^2}\left[\frac{dN_{\alpha\beta}(r)}{dr}\right] \qquad (2)$$

where ρ_β is the number density of β ions and $N_{\alpha\beta}$ is the mean number of β-type ions around α ions at distance r.

The structural results of liquid MgCl$_2$-KCl are described by the RDFs of Mg—Cl, Mg—Mg, Cl—Cl, K—Cl, and K—K as illustrated in Fig. 3. Table 1 displays our calculated values of the first peak positions at an average temperature of 1073 K with varying concentrations of MgCl$_2$ ranging from 22.22 to 80.00 mol%. The first peak positions for Mg—Cl, K—Cl, and Cl—Cl are 2.342, 3.092 and 3.903 Å, respectively, with 22.22% MgCl$_2$ in the binary mixture. With the increasing MgCl$_2$ concentrations, the first peak positions of Mg—Cl pairs are relatively constant over the concentration range studied. Rather, the peaks shift markedly with composition in the case of K—Cl and Cl—Cl pairs. For the 80.00% MgCl$_2$ mixture, the first peak positions of Mg—Cl, K—Cl, and Cl—Cl pairs became 2.343, 3.232, and 3.648 Å. The changes of peak positions of K—Cl, Cl—Cl pairs can be explained that small and doubly charged Mg^{2+} can compete more favorably for the Cl$^-$ compared with K$^+$ and
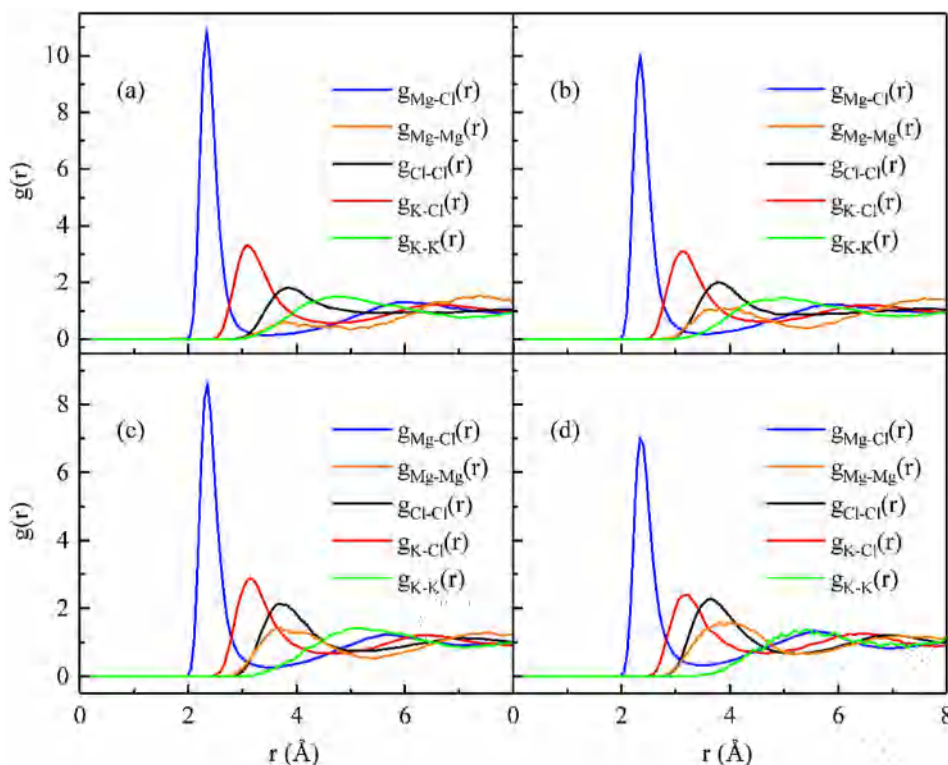

Fig. 3. Radial distribution functions RDFs for Mg—Cl, Mg—Mg, Cl—Cl, K—Cl, and K—K pairs form our FPMD simulations for MgCl$_2$-KCl mixtures at 1073 K. The mole fractions of MgCl$_2$ for (a), (b), (c), and (d) are 22.22%, 33.33%, 50.00%, and 80.00%, respectively.

Table 1
The first peak positions R in the MgCl₂-KCl mixtures estimated from MD and derived from the literature.

Systems (mol%)	T(K)	Method	R_{Mg-Cl}(Å)	R_{K-Cl}(Å)	R_{Cl-Cl}(Å)	Reference
KCl-22.22%MgCl₂	1073	FPMD	2.342	3.092	3.903	This work
KCl-33.33%MgCl₂			2.344	3.156	3.781	
KCl-50.00%MgCl₂			2.357	3.153	3.704	
KCl-80.00%MgCl₂			2.343	3.232	3.648	
100%MgCl₂	1000	FPMD	2.353	–	3.632	Ref [20]
	998	ND[a]	2.420	–	3.560	Ref [40]
100%KCl	1043	MD	–	2.960	4.580	Ref [15]

[a] ND in this paper is an abbreviation for neutron diffraction.

therefore the addition of MgCl₂ to the MgCl₂-KCl mixtures will lead to a decrement of Cl—Cl distance and increment of K—Cl distance. From Fig. 3, it can be seen that the position of the first peak in $g_{Mg-Mg}(r)$ is roughly the same as that in $g_{Cl-Cl}(r)$. This has also been observed in pure MgCl₂ and is attributed to the polarization effect, which allows for an adjustment of the distance between Mg²⁺ cations to approximately equal to that between Cl⁻ anions.

To the best of our knowledge, there are no available experimental data on the nearest-neighbor positions for MgCl₂-KCl melts. Even so, our computed values of R_{Mg-Cl} and R_{K-Cl} in the MgCl₂ richest composition and the KCl richest composition are very close to that of pure melts from the literature [15,20,40], which supports, at least in part, the validity of our calculations.

3.2.2. Average coordination number and neighbor distribution

The average coordination number (CN) and neighbor distribution are calculated to gain further insight into the geometrical structure of the MgCl₂-KCl mixture. The CN is defined as the mean number of β-type ions lying in a sphere of radius R_{min} centered on an α-type ion and it can be evaluated through the following equation:

$$N_{\alpha\beta} = 4\pi\rho_\beta \int_0^{R_{min}} g_{\alpha\beta}(r)r^2 dr \qquad (3)$$

where R_{min} is the position of the first peak valley of the RDF.

Table 2 shows the average coordination numbers (CNs) of Mg—Cl in liquid MgCl₂-KCl mixture with different MgCl₂ mole fractions. With the increase of MgCl₂ concentration, the average coordination numbers for Mg²⁺ ions changes from approximately 4.215 to 4.784, which provided a preliminary prediction that the Mg²⁺ ions accommodated within the Cl⁻ tetrahedral. Further, the probability distribution of coordination numbers of Mg²⁺ ion is shown in Fig. 4. It can be seen that most of the Mg²⁺ ions accommodated within the Cl⁻tetrahedral in the KCl richer concentrations, substantiating the conclusion of several other investigations [2,3,41]. Besides, the population of 4-fold coordination decreases and the population of the 5-fold coordination increases with increasing MgCl₂ concentration, giving an explanation of the increment of the average CN. We note that, even though there is an underestimation of the fraction of 4-coordinated Mg²⁺ cations compared to the experimental data obtained by Raman spectroscopy [3], the trend of our FPMD data and Raman result shows a good coincidence (as presented by the Fig. 4).

Table 2
The coordination numbers and neighbor distribution in the MgCl₂-KCl mixture at 1073 K at various MgCl₂ concentrations.

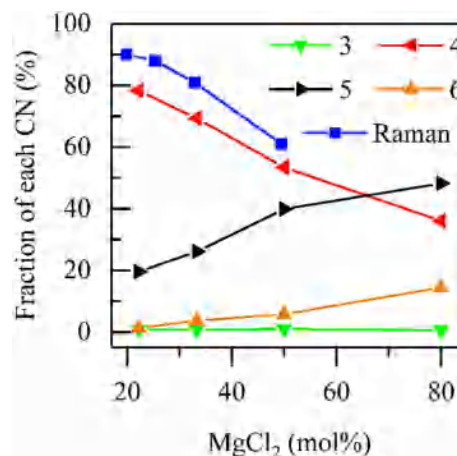| Systems (mol%)	CN = 3	CN = 4	CN = 5	CN = 6	CN = 7	Average
KCl-22.22%MgCl₂	0.785	78.301	19.557	1.356	0.000	4.215
KCl-33.33%MgCl₂	0.750	69.365	26.137	3.698	0.050	4.329
KCl-50.00%MgCl₂	0.929	53.376	39.907	5.752	0.036	4.506
KCl-80.00%MgCl₂	0.600	36.093	48.224	14.482	0.600	4.784

Fig. 4. Fraction of each coordination number of Cl around Mg in the MgCl₂-KCl mixture of different MgCl₂ mole fractions.

3.2.3. Bond angle distributions

To further describe the local structure of molten alkali chloride salts the bond angle distribution of Cl-Mg-Cl, which can reflect the bond orientation, has also been analyzed. As is done in literature [42,43], the bond angle distribution is normalized by $\sin(\theta)$ in this paper to accurately represent the bond angle probability, especially near $\theta = 180°$. We should note that the "bond" in this paper does not mean real covalent bonds, just hypothetical lines connecting near neighbor ion pairs, for example, an Mg—Cl pair.

As shown in Fig. 5, when the initial MgCl₂ concentration changes from 22.22 to 80.00 mol%, the position of the most notable peak of the Cl-Mg-Cl bond angle distribution decreases from 103 to 91°, gradually away from the ideal value of 109.47° for a perfect tetrahedron with the MgCl₂ concentration. In addition, a relatively low peak appears at about 170° over a MgCl₂ concentration range of 50 to 80.00%, and, however, it disappears when the mole fraction of MgCl₂ is less than 33.33%. Further, the R_{Cl-Cl}/R_{Mg-Cl} ratios are 1.667, 1.613, 1.571, and 1.557 with MgCl₂ concentrations of 22.22, 33.33, 50.00, and 80.00 mol%, respectively. The ratios of 1.667 and 1.613 are close to the value of $(8/3)^{1/2} = 1.633$ for a regular tetrahedral, and the ratios of 1.571 and 1.557 are about halfway between that for regularly tetrahedral and octahedral ($2^{1/2} = 1.414$). These results indicate a gradual change in the local geometry of the Mg²⁺ cation in the mixtures. And it is reasonable to infer that the geometry structure of Mg²⁺ coordination shells has changed from a mainly tetrahedral to a distorted octahedral (with vacancies) with the
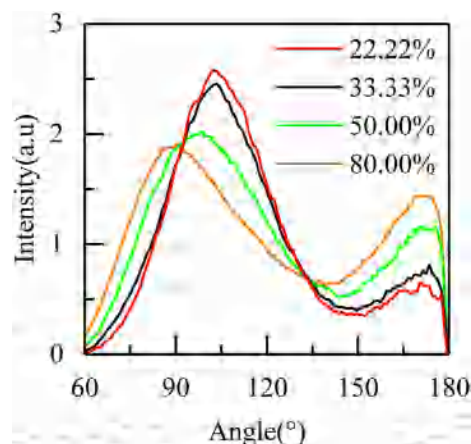

Fig. 5. Bond angle distributions for Cl-Mg-Cl in the MgCl₂-KCl mixtures at multiple MgCl₂ concentrations.

5

addition of MgCl₂. Examples of distorted octahedral with one or two Cl-missing and distorted tetrahedral are presented in Fig. S4 and Fig. S5 to support our opinion. It is worth mentioning that there is some intensity at 180° in the reverse Monte Carlo study of pure MgCl₂ [44]. Nevertheless, this does not affect our conclusion that the local geometry of the Mg²⁺ cation has changed since the positions of the second peaks are very close to 180°.

3.3. Stability and lifetime of Mg—Cl bond

3.3.1. Stability of the Mg—Cl bond

It is not absolutely certain that a higher peak or shorter distance between anion-cation pairs leads to a more stable cation-anion bond. Therefore, the barrier of an anion leaving its central cation is estimated using the potential mean force (PMF), which gives an intuitive comparison of the stability of the cation-anion bond. The PMF can be evaluated from the following equation [45,46]

$$\beta W_{ij}^{eff}(r) = -\ln g_{ij}(r) - 2\ln(r) \tag{4}$$

where $\beta = 1/K_B T$, $W_{ij}^{eff}(r)$ is the effective interaction potential of i and j atoms, and $g_{ij}(r)$ is the corresponding partial RDF. The height between the first minimum and the following maximum corresponds to the barrier of a Cl⁻ anion escape from the coordination shell of the central Mg²⁺ cation. Remarkably, the Mg—Cl barriers, as emphasized in Fig. 6, decreased with the MgCl₂ concentrations, giving evidence of the decreasing Mg—Cl bond stability.

3.3.2. Lifetime of the Mg—Cl bond

The cage correlation function(CCF) is employed to evaluate the time scale of the exchange of Cl⁻ anions between the Mg²⁺ coordination shell and the environment. The cage correlation function is defined as below [19,47].

$$C^{out}(t) = \frac{1}{N_{Mg^{2+}}}\left\langle \sum_1^{N_{Cl^-}} \Theta(1-n_i^{out}(0,t)) \right\rangle \tag{5}$$

where Θ is the Heaviside step function. The lifetime is evaluated as the time for which the cage correlation function takes the value of 1/e, as conducted in the previous literature [48,49].
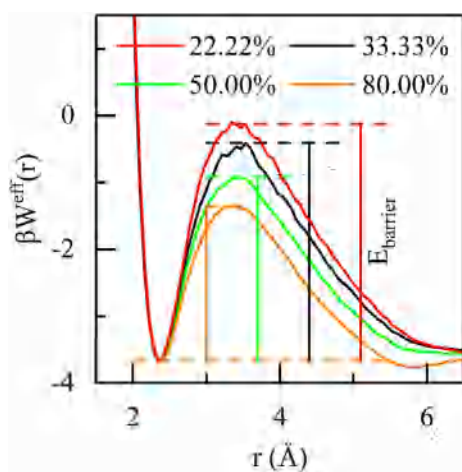

Fig. 6. The potential of the mean force to break the Mg—Cl bond for each composition at 1073 K. The barriers correspond to 22.22, 33.33, 50.00, and 80.00 mol% MgCl₂ concentrations are marked in red, black, green, and orange lines, respectively. All the curves were aligned to the same height at the first minimum of KCl-22.22%MgCl₂. (For interpretation of the references to colour in this figure legend, the reader is referred to the web version of this article.)

Fig. 7 shows the Mg—Cl cage correlation functions for MgCl₂-KCl at multiple MgCl₂ concentrations. The lifetime of the Mg—Cl bond is approximately 13 to 14 ps when the mole fraction of MgCl₂ is less than 50.00% and it decreases to 6.2 and 4.1 ps when the mole fraction of MgCl₂ increases to 50.00 and 80.00%. It seems that the lifetime of the Mg—Cl bond in the KCl-33.33%MgCl₂ system is slightly longer than that in the KCl-22.22% MgCl₂ system, as shown in Fig. 7. However, we doubt this since there is a larger barrier when Cl⁻ anions escape from the coordination shell of Mg²⁺ cations in the KCl-22.22% MgCl₂ system and speculate that this may be caused by the small amount of Mg cations. The decreased lifetime of the Mg—Cl bond is consistent with the decreased Mg—Cl bond stability, indicating that the Mg—Cl coordination shell is less stable and more dynamic at high MgCl₂ concentration.

3.4. Evolution of the network structures

The network structure is analyzed by classifying the Mg—Cl clusters in MgCl₂-KCl into different numbers of Mg cations connected by the sharing of Cl anions. A Mg cation is considered linked to another if it is closer than the position of the first minimum in the Mg—Mg radial distribution function (Fig. 3). As illustrated in Fig. 8 and Fig. S6, the population of Mg—Cl monomer is decreased, whereas the population of Mg—Cl polymer is increased with the addition of MgCl₂ to the mixture. In other words, the addition of MgCl₂ will inhibit the formation of isolated structural units and promote the extension of Mg chains. The monomer is the main species for the Mg ions at the lowest MgCl₂ concentration. Subsequently, the polymers begin to dominate when the concentration of MgCl₂ is above 50%. Eventually, essentially all Mg²⁺ cations are bridged by Cl⁻ anions and forming a network. Besides, it is suggested that there is an equilibrium between the monomers and the dimers in the KCl richer compositions, which is also pointed out by Dai [50].

4. Conclusions

First-principles molecular dynamics simulations are used to explore the effects of MgCl₂ concentration on the microstructural evolution of the KCl-MgCl₂ system. In conclusion, the local geometry of the Mg²⁺ cations, dynamics of Mg²⁺ first coordination shell, and the formation of the network in the KCl-MgCl₂ mixtures are to some extent affected by the ratio of MgCl₂.Based on the obtained results and analyses, tentative conclusions can be drawn as follows:
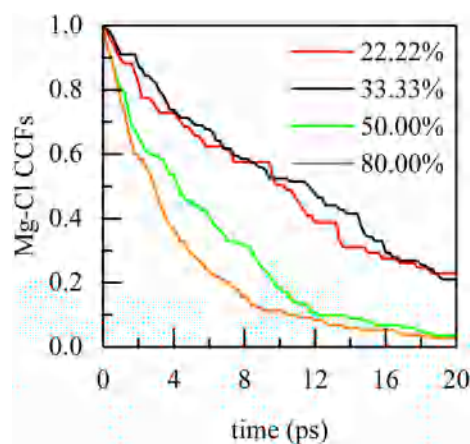

Fig. 7. Mg—Cl cage correlation functions for the MgCl₂-KCl mixture at multiple MgCl₂ concentrations. The Mg—Cl cage correlation functions correspond to 22.22, 33.33, 50.00, and 80.00 mol% MgCl₂ concentrations are marked in red, black, green, and orange, respectively. (For interpretation of the references to colour in this figure legend, the reader is referred to the web version of this article.)
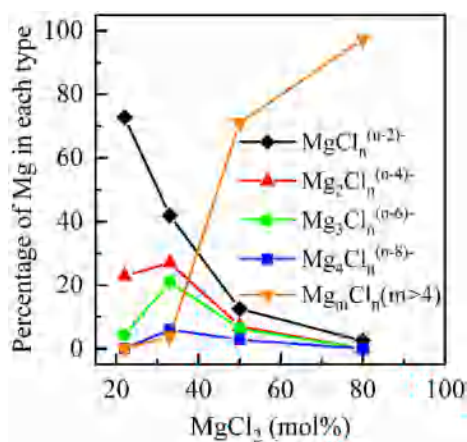
Fig. 8. Percentage of Mg ions involved in various species as a function of $MgCl_2$ concentration.

1. The local geometry of the Mg^{2+} cations converts from mainly tetrahedral to a distorted octahedral geometry with anion vacancies as the concentration of $MgCl_2$ is increased.

2. The coordinated Cl^- anions in Mg^{2+} first coordination shell is more dynamic in $MgCl_2$ richer compositions.

3. The addition of $MgCl_2$ will inhibit the formation of isolated structural units and promote the extension of Mg chains.

In conclusion, FPMD simulations are confirmed to be a useful way of predicting the structural characteristics of molten salt. It can eventually contribute to the design of the electrolyte formula. This work is a preliminary exploration and follow-up work of ternary Mg-based molten salts is in progress.

CRediT authorship contribution statement

Wenshuo Liang: Conceptualization, Data curation, Formal analysis, Investigation, Methodology, Validation, Visualization, Writing - original draft, Writing - review & editing, Software. **Guimin Lu:** Funding acquisition, Resources, Supervision. **Jianguo Yu:** Resources, Supervision.

Declaration of competing interest

None.

Acknowledgments

Appendix A. Supplementary data

Supplementary data to this article can be found online at https://doi.org/10.1016/j.molliq.2020.113131.

References

[1] Y. Zhang, Electrolytic Metallurgy of Magnesium, Central South University, Changsha, China, 2006.

[2] V.A. Maroni, Vibrational Frequencies and Force Constants for Tetrahedral MgX_4^{-2} (X=Cl, Br, and I) in MgX_2–KX Melts, J. Chem. Phys. 55 (1971) 4789–4792.

[3] M.H. Brooker, C.H. Huang, Raman spectroscopic studies of structural properties of solid and molten states of the magnesium chloride – alkali metal chloride system, Can. J. Chem. 58 (1980) 168–179.

[4] N. Galamba, B.J. Costa Cabral, First principles molecular dynamics of molten NaCl, J Chem Phys 126 (2007) 124502.

[5] A. Bengtson, H.O. Nam, S. Saha, R. Sakidja, D. Morgan, First-principles molecular dynamics modeling of the LiCl–KCl molten salt system, Comput. Mater. Sci. 83 (2014) 362–370.

[6] H.O. Nam, A. Bengtson, K. Vörtler, S. Saha, R. Sakidja, D. Morgan, First-principles molecular dynamics modeling of the molten fluoride salt with Cr solute, J. Nucl. Mater. 449 (2014) 148–157.

[7] A.Q. Alsayoud, M. Venkateswara Rao, A.N. Edwards, P.A. Deymier, K. Muralidharan, B.G. Potter Jr., et al., Structure of $ZnCl_2$ melt. Part I: Raman spectroscopy analysis driven by Ab initio methods, J. Phys. Chem. B. 120 (2016) 4174–4181.

[8] X. Li, J. Song, S. Shi, L. Yan, Z. Zhang, T. Jiang, et al., Dynamic Fluctuation of U(3+) Coordination Structure in the Molten LiCl-KCl Eutectic via First Principles Molecular Dynamics Simulations, J. Phys. Chem. A. 121 (2017) 571–578.

[9] J. Song, S. Shi, X. Li, L. Yan, First-principles molecular dynamics modeling of UCl_3 in LiCl-KCl eutectic, J. Mol. Liq. 234 (2017) 279–286.

[10] P. Lucas, G.J. Coleman, M. Venkateswara Rao, A.N. Edwards, C. Devaadithya, S. Wei, et al., Structure of $ZnCl_2$ melt. Part II: fragile-to-strong transition in a tetrahedral liquid, J. Phys. Chem. B. 121 (2017) 11210–11218.

[11] X. Lv, Z. Han, J. Chen, L. Jiang, Z. Xu, Q. Liu, First-principles molecular dynamics study of ionic structure and transport properties of $LiF-NaF-AlF_3$ molten salt, Chem. Phys. Lett. 706 (2018) 237–242.

[12] X. Lv, Z. Han, C. Guan, L. Jiang, S. Wu, Ionic micro-structure and transport properties of low-temperature aluminium electrolytes containing potassium cryolite and sodium cryolite, Phys. Chem. Chem. Phys. 21 (2019) 16573–16582.

[13] X. Lv, Z. Han, H. Zhang, Q. Liu, J. Chen, L. Jiang, Ionic structure and transport properties of KF-NaF-AlF3 fused salt: a molecular dynamics study, Phys. Chem. Chem. Phys. 21 (2019) 7474–7482.

[14] B. Li, S. Dai, Jiang D-e, First-principles molecular dynamics simulations of UCl_n–NaCl (n = 3, 4) molten salts, ACS Appl. Energy Mater. 2 (2019) 2122–2128.

[15] J. Wang, Z. Sun, G. Lu, J. Yu, Molecular dynamics simulations of the local structures and transport coefficients of molten alkali chlorides, J. Phys. Chem. B. 118 (2014) 10196–10206.

[16] J. Wang, J. Wu, Z. Sun, G. Lu, J. Yu, Molecular dynamics study of the transport properties and local structures of molten binary systems (Li, Na)Cl, (Li, K)Cl and (Na, K)Cl, J. Mol. Liq. 209 (2015) 498–507.

[17] J. Wang, J. Wu, G. Lu, J. Yu, Molecular dynamics study of the transport properties and local structures of molten binary alkali metal chlorides. Part III. Four binary systems LiCl-RbCl, LiCl-CsCl, NaCl-RbCl and NaCl-CsCl, J. Mol. Liq. 238 (2017) 236–247.

[18] J. Wu, J. Wang, H. Ni, G. Lu, J. Yu, The influence of NaCl concentration on the (LiCl-KCl) eutectic system and temperature dependence of the ternary system, J. Mol. Liq. 253 (2018) 96–112.

[19] J. Wu, H. Ni, W.S. Liang, G.M. Lu, J.G. Yu, Molecular dynamics simulation on local structure and thermodynamic properties of molten ternary chlorides systems for thermal energy storage, Comput. Mater. Sci. 170 (2019).

[20] W. Liang, J. Wu, H. Ni, G. Lu, J. Yu, First-principles molecular dynamics simulations on the local structure and thermo-kinetic properties of molten magnesium chloride, J. Mol. Liq. 298 (2020).

[21] G. Kresse, J. Furthmüller, Efficient iterative schemes forab initiototal-energy calculations using a plane-wave basis set, Phys. Rev. B. 54 (1996) 11169–11186.

[22] G. Kresse, J. Furthmüller, Efficiency of ab-initio total energy calculations for metals and semiconductors using a plane-wave basis set, Comput. Mater. Sci. 6 (1996) 15–50.

[23] J.P. Perdew, K. Burke, M. Ernzerhof, Generalized gradient approximation made simple [Phys. Rev. Lett. 77, 3865 (1996)], Phys. Rev. Lett. 78 (1997)(1396-1396).

[24] P.E. Blöchl, Projector augmented-wave method, Phys. Rev. B. 50 (1994) 17953–17979.

[25] G. Kresse, D. Joubert, From ultrasoft pseudopotentials to the projector augmented-wave method, Phys. Rev. B. 59 (1999) 1758–1775.

[26] L. Martinez, R. Andrade, E.G. Birgin, J.M. Martinez, PACKMOL: a package for building initial configurations for molecular dynamics simulations, J. Comput. Chem. 30 (2009) 2157–2164.

[27] F. Birch, Finite elastic strain of cubic crystals, Phys. Rev. 71 (1947) 809–824.

[28] F.D. Murnaghan, The compressibility of media under extreme pressures, Proc. Natl. Acad. Sci. U. S. A. 30 (1944) 244–247.

[29] S. Grimme, Accurate description of van der Waals complexes by density functional theory including empirical corrections, J. Comput. Chem. 25 (2004) 1463–1473.

[30] S. Grimme, Semiempirical GGA-type density functional constructed with a long-range dispersion correction, J. Comput. Chem. 27 (2006) 1787–1799.

[31] S. Le Roux, P. Jund, Ring statistics analysis of topological networks: new approach and application to amorphous GeS_2 and SiO_2 systems, Comput. Mater. Sci. 49 (2010) 70–83.

[32] N. Michaud-Agrawal, E.J. Denning, T.B. Woolf, O. Beckstein, MDAnalysis: a toolkit for the analysis of molecular dynamics simulations, J. Comput. Chem. 32 (2011) 2319–2327.

[33] D.T. Cromer, J.B. Mann, X-ray scattering factors computed from numerical Hartree–Fock wave functions, Acta Crystallographica Section A 24 (1968) 321–324.

[34] F. Wu, S. Roy, A.S. Ivanov, S.K. Gill, M. Topsakal, E. Dooryhee, et al., Elucidating ionic correlations beyond simple charge alternation in molten $MgCl_2$-KCl mixtures, J. Phys. Chem. Lett. (2019) 7603–7610.

[35] J.N. Reding, Densities and molal volumes of molten magnesium chloride, potassium chloride, and barium chloride mixtures, J. Chem. Eng. Data. 10 (1965) 1–4.

[36] K. Grjotheim, J.L. Holm, B. Lillebuen, H.A. Øye, Densities and excess molar volumes of binary and ternary melts of $MgCl_2$, $CaCl_2$ and AlkCl, Trans. Faraday Soc. 67 (1971) 640–648.

[37] M. Parrinello, A. Rahman, Crystal structure and pair potentials: a molecular-dynamics study, Phys. Rev. Lett. 45 (1980) 1196–1199.

[38] M. Parrinello, A. Rahman, Polymorphic transitions in single crystals: a new molecular dynamics method, J. Appl. Phys. 52 (1981) 7182–7190.

[39] T. Bucko, F. Simko, Effect of alkaline metal cations on the ionic structure of cryolite melts: ab-initio NpT MD study, J Chem Phys 148 (2018), 064501.

[40] S. Biggin, M. Gay, J.E. Enderby, The structures of molten magnesium and manganese (II) chlorides, J. Phys. C. Solid State Phys. 17 (1984) 977–985.

[41] V.A. Maroni, E.J. Hathaway, E.J. Cairns, Structural studies of magnesium halide-potassium halide melts by Raman spectroscopy, J. Phys. Chem. 75 (1971) 155–159.

[42] M.G. Tucker, D.A. Keen, J.S. Evans, M.T. Dove, Local structure in ZrW(2)O(8) from neutron total scattering, J Phys Condens Matter 19 (2007), 335215.

[43] A. Zeidler, P.S. Salmon, R.A. Martin, T. Usuki, P.E. Mason, G.J. Cuello, et al., Structure of liquid and glassy ZnCl$_2$, Phys. Rev. B 82 (2010).

[44] L. Pusztai, R.L. McGreevy, The structure of molten ZnCl$_2$ and MgCl$_2$, J. Phys-Condens. Mat. 13 (2001) 7213–7222.

[45] M. Levesque, V. Sarou-Kanian, M. Salanne, M. Gobet, H. Groult, C. Bessada, et al., Structure and dynamics in yttrium-based molten rare earth alkali fluorides, J Chem Phys 138 (2013), 184503.

[46] S. Wang, S. Xiao, W. Hu, H. Deng, Effect of MCl$_3$ (M=La, U or Sc) component on the local structures and transport properties of LiCl–KCl–MCl$_3$ eutectic: a molecular dynamics study, Electrochimica Acta 306 (2019) 366–376.

[47] E. Rabani, J.D. Gezelter, B.J. Berne, Calculating the hopping rate for self-diffusion on rough potential energy surfaces: cage correlations, J. Chem. Phys. 107 (1997) 6867–6876.

[48] M. Salanne, C. Simon, P. Turq, R.J. Heaton, P.A. Madden, A first-principles description of liquid BeF2 and its mixtures with LiF: 2. Network formation in LiF-BeF$_2$, J. Phys. Chem. B 110 (2006) 11461–11467.

[49] B. Morgan, P.A. Madden, Ion mobilities and microscopic dynamics in liquid (Li,K)Cl, J Chem Phys 120 (2004) 1402–1413.

[50] S. Dai, G.M. Begun, J.P. Young, G. Mamantov, Application of chemometric methods in Raman spectroscopic studies of molten salt system containing MgCl2-KCl: experimental evidence for existence of Mg2Cl73− dimer and its Raman spectrum, J. Raman Spectrosc. 26 (1995) 929–932.